RSC Advances

This is an *Accepted Manuscript*, which has been through the Royal Society of Chemistry peer review process and has been accepted for publication.

Accepted Manuscripts are published online shortly after acceptance, before technical editing, formatting and proof reading. Using this free service, authors can make their results available to the community, in citable form, before we publish the edited article. This *Accepted Manuscript* will be replaced by the edited, formatted and paginated article as soon as this is available.

You can find more information about *Accepted Manuscripts* in the Information for Authors.

Please note that technical editing may introduce minor changes to the text and/or graphics, which may alter content. The journal's standard Terms & Conditions and the Ethical guidelines still apply. In no event shall the Royal Society of Chemistry be held responsible for any errors or omissions in this *Accepted Manuscript* or any consequences arising from the use of any information it contains.

ROYAL SOCIETY OF CHEMISTRY

www.rsc.org/advances

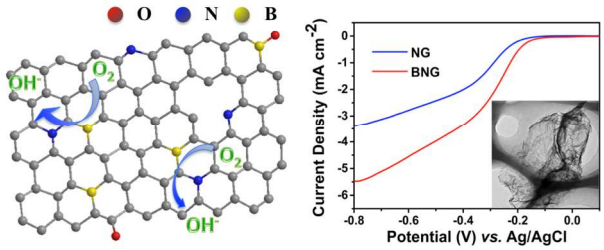

Boron and nitrogen co-doped graphene was synthesized as synergistically enhanced catalyst for oxygen reduction reaction *via* a two-step doping strategy.

RSC Advances Accepted Manuscript

RSC Advances

RSCPublishing

ARTICLE

Two-step synthesis of boron and nitrogen co-doped graphene as synergistically enhanced catalyst for oxygen reduction reaction

Cite this: DOI: 10.1039/x0xx00000x

Received 00th January 2012,
Accepted 00th January 2012

DOI: 10.1039/x0xx00000x

www.rsc.org/

Jiapo Tai[a†], Jiantong Hu[a†], Zhongxin Chen[a] and Hongbin Lu*[a]

A two-step strategy was developed to co-dope graphene with boron and nitrogen as a metal-free catalyst for oxygen reduction reaction (ORR). This method involved a hydrothermal reaction and a thermal annealing procedure, which guaranteed the efficient insertion of heteroatoms, producing B and N co-doped graphene frameworks (BNG) with high ORR reactivity, good stability and tolerance for methanol in alkaline media. The onset potential of BNG was -0.17 V, and the current density reached -5.5 mA cm^{-2} at the voltage of -0.8 V during the RDE test (*vs.* Ag/AgCl, rotating rate = 1600 rpm, scanning rate = 10 mV s^{-1}), comparable to high-performance commercial Pt/C catalyst. It is believed that the superior catalytic reactivity arises from the synergistic coupling of B and N dopants on the graphene domains.

RSC Advances Accepted Manuscript

Introduction

The past few decades has witnessed a tremendous growth in energy demand. Seeking economic, abundant and clean power sources has been the focus of plenty of efforts.[1] Fuel cells based on the oxygen reduction reaction (ORR) are deemed to be a promising solution to the energy crisis in view of their high-efficiency and zero-emission.[2]

ORR catalysts are generally based on noble metals such as Pt and its alloys.[3-4] Despite the adorable catalytic activity, however, the limited reserve of noble metals, their durability in corrosive environments and the poor tolerance for methanol had largely hindered the practical application.[5-7] By comparison, carbon-based materials, or named "metal-free" catalysts, are cost-effective, highly stable and free from the catalyst deactivation.[8-9] Among all the metal-free ORR catalysts, graphene has great potential due to its high specific surface areas, extraordinary electrical conductivity and prominent mechanical and chemical stability.[10]

Pristine graphene is a zero bandgap material that hardly exhibits any ORR reactivities,[11] but its catalytic performance can be massively improved by heteroatom doping, such as nitrogen, boron, sulphur, iodine and phosphor.[12-16] This dramatically enhanced activity is believed to arise from the insertion of heteroatoms into sp^2-hybridized carbon frameworks, which breaks the electroneutrality between carbon and dopant, and creates charged sites favourable for the surface adsorption of O_2.[2,17]

There have been numerous efforts dedicated to investigating metal-free catalysts. Dai *et al.* first synthesized N-doped carbon nanotubes and indicated that the positively charged carbon atoms adjacent to nitrogen dopants were the active centers.[18] Wu *et al.* and Zheng *et al.* prepared the N-doped graphene by hydrothermal reaction of graphite oxide (GO) with urea, suggesting that the remarkable ORR activity was related to the abundance and various types of N atoms contained.[19-20] Sheng *et al.* confirmed that the electrocatalytic ability of B-doping was a result of electron accumulation in the vacant 2p orbital of the boron dopant. The B atoms transferred electrons to the chemically adsorbed O_2 molecules, weakening the O-O bonds and facilitating the ORR.[9] It comes naturally to a question whether co-doping graphene with B and N could offer a further enhanced performance, and the discovery of Yu *et al.* indicated that a B and N separated structure can also turn the inert graphene domain into active.[21]

Nevertheless, the previous reports have not yet drawn an end to the issue of co-doping. Recent studies have revealed the existence of a synergistic coupling effect, predicting that a B-C-N heteroring, especially where a B atom is *meta* to a pyridinic N, would offer much more active performance than singly doped ones.[22] Along with the assertion that the hexagonal boron

nitride (*h*-BN) formed in most of the one-step co-doping strategies hampers the ORR process,[23] Wang *et al.* deliberately prepared B and N isolate-doped graphene nanosheets, and showed an appealing performance.[24] These practices have indicated clearly a direction to further exploit the ORR potential of B and N co-doped graphene.

In order to prepare desired doped samples, we propose a new, two-step synthesis strategy. In the first step, the hydrothermal reaction of graphite oxide (GO) with urea is used to produce precursors with sufficient N atoms, donated as NG.[25] Subsequently, NG is mixed with boric acid and thermally annealed in argon to produce B and N co-doped graphene, donated as BNG. Different from the reported co-doping strategies, our method does not require harsh and potentially hazardous conditions, for example, annealing the precursor with ammonia.[22-23] Neither do we have to use/release expensive and toxic reagents during the whole process such as cobalt chloride and borane complexes.[15,26] This makes the present synthesis strategy cost-effective, environmental friendly, and promises to be used in practical applications.

We characterize the electrocatalytic property of BNG in alkaline media, which exhibits excellent ORR reactivity, good durability and tolerance for methanol. The special B-C-N heterorings on the BNG surface are believed to be the origin of the synergistic effect between B and N, which results in an enhanced performance of this catalyst. Meanwhile, the N-containing precursor with low oxygen content would be more favourable for effective B-doping process, given that the oxygen functional groups may affect the binding state of B, thereby decreasing the efficiency of dual-doped catalyst. We believe that these findings would be helpful for achieving the rational design of co-doped graphene catalysts.

Experimental Section

Chemicals

Graphite powder 8099200 (120 μm) was purchased from Qingdao BCSM Co.; 98% H_2SO_4, urea and 30% H_2O_2 were purchased from Sinopharm Chemical Regent Co.; sodium nitrate was purchased from Shanghai Qiangshun Chemical Co.; $KMnO_4$ and ethanol were purchased from Shanghai Zhenxin Chemical Co.; α-Al_2O_3 (0.3 μm) and γ-Al_2O_3 (0.05 μm) were purchased from CH Instruments Inc.; boric acid, Pt/C catalyst 35849 (nominally 20% of Pt loading) and 5 wt% Nafion® solution were purchased from Alfa Aesar. All chemicals were used as received. Deionized (DI) water was used in all the experiments.

Characterizations

Transmission electron microscopy (TEM, JEM-2100F, operating at 200 kV) was used to study the morphology of NG and BNG. All the samples for imaging were prepared by depositing aqueous dispersions (~0.1 mg mL^{-1}) on holey copper grids. Thermogravimetric analysis (TGA) was conducted with Pyris 1 TGA, and nitrogen was used as purge gas. X-ray photoelectron spectra (XPS) were carried out on a PHI Quantera SXM™ scanning X-ray Microprobe™. Raman spectra were conducted on XploRA (HORIBA JobinYvon) laser Raman spectrometer (Wavelength = 532 nm). X-ray diffraction (XRD) was carried out on a PANalytical X'Pert PRO X-ray diffractometer with Cu K_α radiation (λ = 1.54 Å) in 2θ range from 5 to 60 º.

Material Synthesis

Graphite Oxide (GO)

GO was synthesized *via* Hummer's method. 1 g of graphite powder was added into a mixture of 23 ml of 98% H_2SO_4 and 0.75 g of $NaNO_3$, followed by the addition of 3 g of $KMnO_4$. The reactants were kept for 45 min at 35°C. Afterwards, DI water and 10 ml of 30% H_2O_2 were added.

The as-prepared GO was transferred into dialysis bags and kept in DI water for 1 week to remove residual acid. GO was freeze-dried and kept in vacuum.

Nitrogen-doped Graphene (NG)

NG was synthesized *via* hydrothermal reaction of GO in the presence of urea. 0.5 g of GO was first dissolved in 500 ml of DI water and 150 g of urea was subsequently added. The suspension was ultrasonically treated for 2 h to achieve homogeneous dispersion.

The above suspension was then poured into autoclaves, sealed and put into oven to complete the hydrothermal reaction at 180°C. After 12 h, the autoclave was cooled to room temperature.

The product obtained (NG) was filtrated, washed and dialyzed by DI water to remove impurities and finally freeze-dried in vacuum.

Boron, nitrogen co-doped Graphene (BNG)

0.1 g of NG precursor was put into 20 ml of DI water, followed by the addition of 0.5 g H_3BO_3 and ultrasonically dispersed to obtain a suspension. The suspension was then boiled to expel water, resulting in a paste and to be transferred into a crucible.

BNG was obtained *via* annealing the mixture paste under the protection of argon. The heating rate of the process was 10 °C min^{-1} while the final temperature was set at 900 °C and kept for 30 min.

Finally, BNG was put into 100 ml of 80 °C DI water and stirred for 1 h to dissolve the impurities. The product was filtrated, washed, and dried in a 60 °C vacuum oven for 12 h.

Electrode preparation and electrochemical characterizations

All the working electrodes were prepared under the same condition. For instance, when preparing the BNG electrode, 2 mg sample was added into the mixture of 1.8 ml ethanol and 0.2 ml Nafion® D-520 dispersion (5% w/w in water and 1-propanol). The mixture was further homogenized *via* ultrasonication for 2 h, with a concentration of 1 mg ml^{-1}.

Subsequently, 20 μL of the catalyst solution was transferred onto the surface of glassy carbon electrode with a diameter of 5 mm *via* a controlled drop casting approach.

RSC Advances Accepted Manuscript

 This journal is © The Royal Society of Chemistry 2012

The electrochemical characterization was conducted in a three-electrode system, of which the reference electrode is Ag/AgCl in a saturated KCl-AgCl solution and the counter electrode is a platinum foil.

Linear sweep voltammetry (LSVs), cyclic voltammetry (CVs) and rotating disk electrode (RDE) tests were carried out on CHI 605 electrochemical workstation (CHI Inc., United States). The electrolyte is a 0.1 mol L^{-1} KOH solution that had been purged with oxygen/nitrogen. During the whole characterization process, a steady flow of oxygen/nitrogen was used to ensure the continued saturation.

Results and discussion

We synthesize the catalyst following a two-step procedure. Firstly, GO was treated with urea to form NG by a hydrothermal reaction. Subsequently, BNG was prepared through thermally annealing NG with boric acid.

Morphologies of NG and BNG were studied *via* transmission electron microscopy (TEM). As shown in **Fig. 1a**, the slice-like morphology of NG is a result of the exfoliation of GO before the hydrothermal treatment,[26] and the wrinkled and crumpled structure come from the shearing and crushing effect during the hydrothermal treatment.[19] After annealing, the wrinkled morphology remains to be reserved in BNG (**Fig. 1b**).

X-ray photoelectron spectroscopy (XPS) is a powerful tool to characterize the doping levels of heteroatoms. In the wide scan spectra (**Fig. 2a**), the peaks at 400 eV and 192 eV refer to the nitrogen and boron atoms respectively.[27] The atomic percentage of nitrogen was found to be 9.34% in NG precursor and it declined to 6.80% in BNG. Meanwhile, the atomic percentage of boron in BNG was found to be 4.82%, suggesting successful incorporation of B into graphene upon annealing. The peak deconvolution reveals detailed configurations of the dopants, and to minimize its influence, we fixed all fitting parameters according to the literature. The slight variation of full width half maximum (FWHM) in N_{1s} spectra for NG and BNG would not cause significant deviation to the final result. After many times of fitting optimization, the relative error was estimated to be smaller than 10%. (More details of XPS peak deconvolution are presented in **Table S1** in the ESI.)

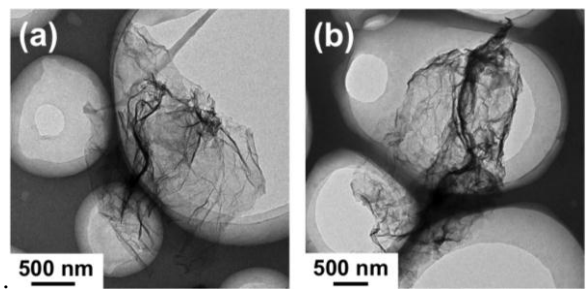

Fig. 1 TEM images of (a) NG and (b) BNG.

The N_{1s} XPS spectra (**Fig. 2b** and **Fig. 2c**) reveal the local chemical binding states and relative contents of different N atoms in the precursor and the final product, namely graphitic (also quaternary), pyrrolic and pyridinic. Graphitic N is a replacement of C atoms in the graphene basal plane that linked with three C atoms in a hexagonal ring; pyrrolic N exists in a five-member ring, donating two p-electrons to the π-conjugated system; pyridinic N occurs in six-member ring on the edges, donating one p-electron to the aromatic system.[28] After thermal treatment, we found that the content of different N atoms in graphene varied obviously. Although the content of pyridinic N remained constant, pyrrolic N decreased from 47.4% in the precursor to 39.9% in BNG while the content of graphitic N increased from 10.8% to 18.8%. This phenomenon can be explained as follows. Among three types of N atoms, graphitic N has the highest thermal stability while the stability of pyrrolic N is the lowest.[20] The relative percentage of pyridinic N species is primarily dependent on two contradictory factors: 1) increase by lowering the content of pyrrolic N; 2) decrease by increasing the content of graphitic N. The interplay between these two factors results in a nearly constant pyridinic N% at 900 °C. The conversion of pyrrolic N to pyridinic and graphitic N may also contribute to this trend, as reported by Lin *et al.*[29] The loss of pyrrolic N in BNG does not decrease the ORR reactivity, because the latter does not seem to relate to the total nitrogen content in N-doped graphene, as suggested by Lai *et al.*[30]

It has been recognized that graphitic N and pyridinic N play critical roles in determining the ORR performance of the material. The former mainly accounts for the conductivity and determines the limiting current density, while the latter leads to the attachment of oxygen and controls the onset potential.[31-33]

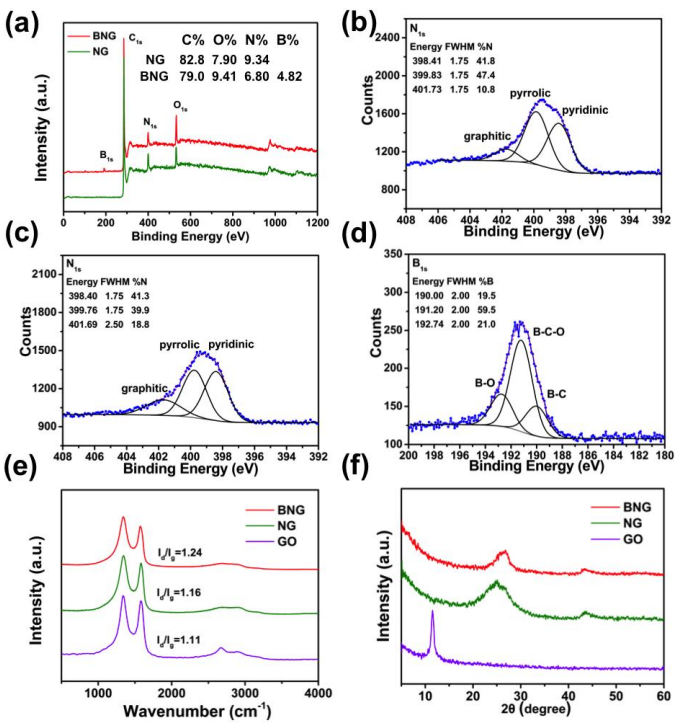

Fig. 2 (a) XPS spectra of NG and BNG; (b) XPS-N_{1s} spectrum of NG; (c) XPS-N_{1s} spectrum of BNG; (d) XPS-B_{1s} spectrum of BNG; (e) Raman spectra of BNG, NG and GO; (f) XRD patterns of BNG, NG and GO.

RSC Advances Accepted Manuscript

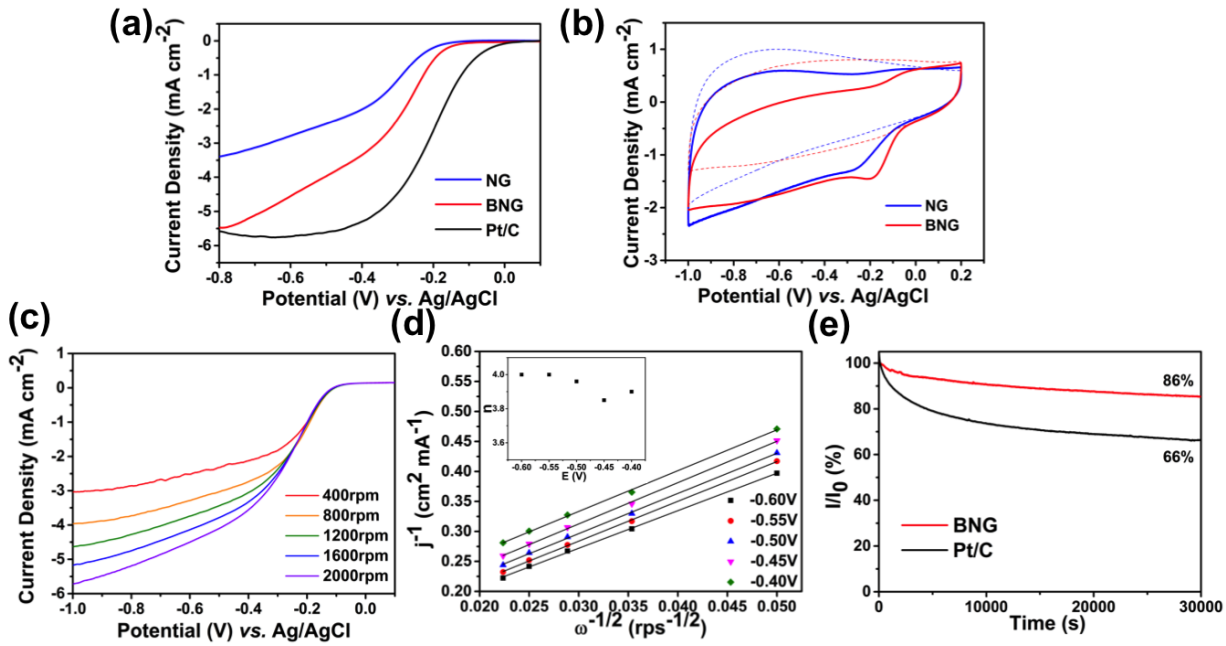

Fig. 3 (a) LSVs of NG, BNG and Pt/C catalyst in O_2-saturated 0.1 mol L^{-1} KOH solution, with the rotating rate of 1600 rpm and scanning rate of 10 mV s^{-1}; (b) CVs of NG and BNG in O_2/N_2-saturated 0.1 mol L^{-1} KOH, where the dash stand for curves in N_2 (scan rate = 100 mV s^{-1}); (c) LSVs of BNG at different rotating rate in O_2-saturated 0.1 mol L^{-1} KOH (scan rate = 10 mV s^{-1}); (d) K-L plots based on RDE data at various potentials and electron transfer numbers per O_2 molecule; (e) chronoamperometric responses of BNG and Pt/C catalyst in O_2-saturated 0.1 mol L^{-1} KOH.

It is also suggested that the catalytic activity for ORR is more dependent on the graphitic N at exposed zigzag edges.[34] Hence, we speculate that the increased level of graphitic N in BNG would promote the ORR performance of doped graphene.

The O_{1s} XPS (See **Fig. S1**) results reveal the existence of B-O bonds (BE = 533.6 eV) in the final product. Yet in the N_{1s} XPS of BNG, compared with NG, there is few evidence that justifies the formation of N-B bonds (BE = 398 eV).[15,22,26] Given the content of oxygen in the NG precursor, as well as the fact that boric acid tends to combine with the unreduced O-containing groups during annealing (eventually will lead to by-products that are hard to be eliminated *via* heat treatment),[26] it is more likely that the B atoms in BNG exist in the form of B-C and B-O bonds instead of *h*-BN. Therefore, we deconvoluted the B_{1s} XPS (**Fig. 2d**) into BC_3 (BE = 190.0 eV), B-C-O (including BC_2O and BCO_2, BE = 191.2 eV), and B-O (BE = 192.7 eV) moieties. As a result, the structure of B-C-N heterorings is very likely to exist in BNG. This is because its major components, B-C and C-N bonds, have already been justified in the XPS spectra while N-B bonds cannot be observed in the N_{1s} spectrum. However, due to the complicated surface chemical states of the dopants, it is hard to determine exactly the binding energy and to distinguish it from different moieties with similar BE values, refer to **Table S2** in the ESI. What's more, it is noted that the efficiency of B-doping was lowered, since many B atoms linked with O atoms did not conjugate with the aromatic π system.

Raman spectra in **Fig. 2e** also provide information to study the structure of the final product. The two remarkable peaks around 1340 and 1580 cm^{-1} referred to the D band and G band of the graphene domain, respectively. D band is related to the sp^3 carbon at defective sites while G band corresponds to the E_{2g} stretching vibration mode of sp^2 carbon.[35] The intensity ratio of I_D to I_G reflects the content of the structural defects. For our sample, it increased from 1.11 to 1.16 after N-doping. Actually this is a result of combining the reduction reaction and the heteroatom insertion. The reduction of GO under hydrothermal conditions tends to decrease the I_D/I_G value while N-doping causes the formation of more defective sites.[19,36] B-doping at high temperatures increases the I_D/I_G ratio to 1.24 because the incorporation of B atoms led to the formation of C-B and O-B bonds, which had different lengths from C-C bond, resulting in the asymmetry of graphene networks.[22] Besides, O-containing groups in the NG precursor also tend to be removed by pyrolysis below 400 °C,[27] causing the formation of more defects. Such a tendency was confirmed by thermal gravimetric analysis (TGA). As shown in **Fig. S2**, after annealing, the BNG became more stable than the precursor NG. Moreover, the XRD patterns (**Fig. 2f**) of both NG and BNG exhibit strong diffraction peaks at 2θ = 25.02 ° and 26.74 °, which can be attributed to the (002) lattice plane of the graphene sheets.[27] Based on these results, the thicknesses of NG and BNG layers are found to be 3.56 Å and 3.33 Å, respectively. The former represents a typical structure of exfoliated, reduced graphene sheets (the NG precursor), while the latter implies that the pyrolysis has caused the dense restacking of graphene sheets, and partial restoration of graphite properties.[15]

Linear sweep voltammetry (LSV) was applied to investigate the ORR performance of the catalyst. Three different kinds of catalysts, namely the NG precursor, BNG and a high-performance commercial Pt/C catalyst were coated on the

RSC Advances Accepted Manuscript

 This journal is © The Royal Society of Chemistry 2012

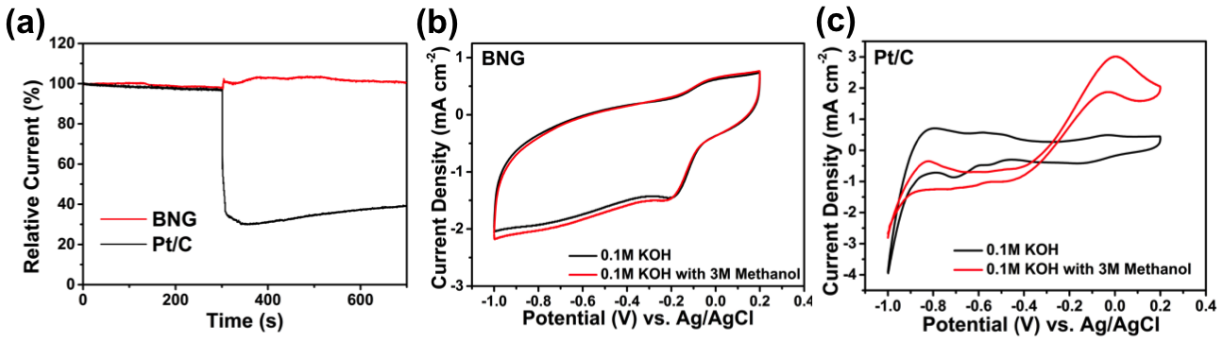

Fig. 4 (a) current-time chronoamperometric of the two catalysts at -0.3 V, when methanol was both added at the 300th second; (b-c) CVs of BNG and commercial Pt/C catalyst with/without the existence of 3 mol L^{-1} methanol (scan rate = 100 mV s^{-1}).

surface of a GC rotating disk electrode. Their ORR properties were tested in a 0.1 mol L^{-1} KOH solution with a rotating rate of 1600 rpm and a scan rate of 10 mV s^{-1}. Apparently, after B-doping, BNG exhibited a significantly improved reactivity, where the limiting diffusion current density at -0.8 V increased from -3.4 to -5.5 mA cm^{-2}. This value is comparable to other reported results (see **Table S3**). The onset potential of BNG was -0.17 V (*vs.* Ag/AgCl), which was not as positive as that of Pt/C (-0.08 V) but still higher than that of NG (-0.21 V).

The results of cyclic voltammetry (scan rate = 100 mV s^{-1}) are shown in **Fig. 3b**. Compared with the CV curve of NG in O_2, BNG's curve had a more positive onset potential, a more obvious oxygen reduction peak and a flatter plateau. This indicates the enhanced ORR reactivity after B-doping.

To further study the corresponding mechanism, we carried out RDE tests at different rotating rates (see **Fig. 3c**). The Koutecky-Levich (K-L) equation was applied to calculate the number of electrons transferred per oxygen molecule:[30]

$$\frac{1}{j} = \frac{1}{j_k} + \frac{1}{B\omega^{1/2}}$$

where j_k is the kinetic current density and ω is the rotating speed (expressed in rpm). The value of B can be expressed as follows:

$$B = 0.2nF(D_{O_2})^{2/3}v^{-1/6}C_{O_2}$$

where n is the electron transfer number per oxygen molecule, F is the Faraday constant (96485 C mol^{-1}), D_{O2} is the diffusion coefficient of oxygen in 0.1 mol L^{-1} KOH (1.9×10^{-5} cm^2 s^{-1}), v is the viscosity of the electrolyte solution (0.01 cm^2 s^{-1}), C_{O2} is the concentration of oxygen dissolved (1.2×10^{-6} mol cm^{-3}).

The K-L plots (j^{-1} *vs.* $\omega^{-1/2}$) at different potentials all exhibit good linearity (**Fig. 3d**). This means that the catalytic mechanism obeys a first-order kinetic with respect to the O_2 concentration. The numbers of electrons transferred per O_2 molecule at various potentials, n, were fitted and also shown in **Fig. 3d**. The values of n, which were larger than 3.8 below -4.0 V, are much higher than that of the NG precursor that was produced through the same hydrothermal reaction ($\approx$ 3.5 at -0.6 V)[19]. This indicates a better selectivity for the efficient $4e^-$ pathway.[37]

The kinetic current density, j_k, is the key to quantitatively evaluating the nature of catalysts. For instance, at -0.6 V, the j_k of BNG equals 12 mA cm^{-2}, being larger than that of both the N-doped graphene (N content = 9.7 at%, $j_k \leqslant 3$ mA cm^{-2})[38] and boric acid-annealed GO (B content = 3.6 at%, $j_k \approx$ 3.5 mA cm^{-2})[22]. Since BNG has a lower N content than the NG precursor, it is impossible to reach such a value by directly adding N-doped graphene and B-doped graphene's j_k values. Meanwhile, it should be emphasized that the overall catalytic activity is not practically a simple superposition between contributions of B and N elements, but also a result of a synergistic effect between them.

To elucidate this, we classify the possible active sites on BNG into two types. The first type belongs to separated N or B atoms in graphene. In this case, both the C atoms close to N atoms and graphitic B atoms are reactive. As long as B is not directly linked with N, the two heteroatoms can preserve their intrinsic ORR activities.[18,21] The second type are B-C-N heterorings. It is studied that especially when a B atom is *meta* to a pyridinic N, the 2p orbital of the C atoms located between N and B can be polarized by N, and allow to donate extra electrons to the adjacent B atom. The B atom is thus "activated" since its electron occupancy is increased and facilitates the adsorption and bonding with O_2.[11,22,24] Calculations related to the energy gap between the highest-occupied molecular orbital (HOMO) and the lowest-unoccupied molecular orbital (LUMO) of graphene are in agreement with this explanation.[23]

Apparently, our two-step synthesis strategy had successfully achieved synergistically improved ORR catalytic properties. However, it should be mentioned that the hydrothermal treatment practically causes a limited reduction of GO, residual oxygen-containing groups still exist in the final product and probably hinder the doping of B to some extent, eventually leading to the formation of inactive B-O structures.

To evaluate the durability of BNG, we compared it with the Pt/C catalyst at a constant voltage of -0.3 V on the disk electrode with a rotating rate of 1000 rpm (see **Fig. 3e**). The result is presented in the form of relative current intensity (I/I_0), which is the ratio of the current density at a certain moment to the initial value. For the commercial Pt/C catalyst, I/I_0 decays rapidly to 66% while BNG exhibits a very slow decline, and after 30000 s still retains 86% of the initial reactivity. Although this durability was not the best one,[39] it was comparable to

RSC Advances Accepted Manuscript

other counterparts.[16,26,27] This could arise from the existence of many ORR-inert oxygen functional groups in BNG. During the test, the elimination of these groups could cause the structural decomposition and damage the durability of the catalyst.

Based on these results, it is apparent that the incorporation of nitrogen and boron atoms affords an effective approach to synergistically improve the ORR reactivity of graphene. Nonetheless, the role of oxygen groups has seldom been involved in this respect. Our results indicate that the oxygen groups might affect the durability and reactivity in an underlying way. Therefore, we suggest that for two-step doping strategies, a precursor with less oxygen groups is expected to be favourable for effective B-doping. Because this will lead to a higher combination degree of BC_3 in the final catalyst, as mentioned in Zheng's study.[22]

For Pt-based ORR catalysts, the poor methanol tolerance has been a limited factor that is hard to overcome. We recorded the current-time relationship of Pt/C and BNG at a potential of -0.3 V in the presence of methanol. In **Fig. 4a**, a mixture of CH_3OH, KOH and H_2O was added into the electrolyte at the 300^{th} second to adjust the concentration of methanol to 3 mol L^{-1}. It is found that although the relative current density of the Pt/C electrode remarkably declined (69%) immediately after methanol addition, the effect of methanol on the reactivity of BNG is negligible.

The result of cyclic voltammetry (CV) also exhibits a similar trend. As shown in **Fig. 4b**, the curve shape of BNG is independent of the existence of methanol, displaying a peak ORR potential around -0.2 V. In contrast, when cycling in methanol, the CV curve of Pt/C (**Fig. 4c**) completely deformed, exhibiting a broad, cross-over peak of methanol oxidation (from -0.4 V to 0 V).[30] This clearly demonstrated a good methanol tolerance of the metal-free catalyst we prepared toward the ORR.

Conclusions

We have proposed a two-step method to prepare N and B co-doped graphene as an effective metal-free ORR catalyst. The synthesis involved a hydrothermal step of GO and urea to prepare NG and an annealing step of the mixture of NG and boric acid to give BNG. The final product BNG exhibited excellent ORR performance and a synergistic improvement effect between N and B. B-C-N heterorings on the BNG surface were deemed to be the origin of this synergisitic effect. In such a structure, the 2p orbital of C atoms located between N and B makes the free flowing of π electrons possible, activating the B atoms to facilitate the surface adsorption of O_2. In addition, we suggest that the content of oxygen in the precursor might influence the second doping step, and diminish the durability and reactivity of the catalyst. The N/B co-doped catalyst showed excellent methanol tolerance and improved durability, which is superior to the commercial Pt/C catalyst. Compared with other synthetic methods, our approach requires only common chemicals, nontoxic precursors and relatively mild reaction conditions, is thus cost-effective and environmental friendly. The high performance and excellent stability of BNG make it a promising catalyst for ORR in alkaline fuel cells.

Acknowledgements

We are grateful to Mr. Wenbin Cai and his research team (Fudan University) for the assistance with electrochemical characterizations. We also thank Ms. Xiaoyan Ye (Tsinghua University Analysis Centre) for XPS characterizations. This work is supported by National Basic Research Program of China (grant no. 2011CB605702), NSF of China (grant no. 50573014, 50773012 and 51173027), Shanghai Nanotechnology Program (grant no. 1052nm00400) and Shanghai Basic Research Program (grant no. 14JC1400600).

Notes and references

[a] State Key Laboratory of Molecular Engineering of Polymers, and Department of Macromolecular Science, Fudan University, 220 Handan Road, Shanghai, 200433, China. Tel/Fax: 86-21-5566 4589; Email: hongbinlu@fudan.edu.cn.

† These authors contributed equally to the work.

1 Y. Liang, Y. Li, H. Wang, J. Zhou, J. Wang, T. Regier and H. Dai, *Nat. Mater.*, 2011, **10**, 780-786.
2 X. Zhou, J. Qiao, L. Yang and J. Zhang, *Adv. Energy Mater.*, 2014, **4**.
3 B. B. Xiao, X. Y. Lang and Q. Jiang, *RSC Adv.*, 2014, **4**, 28400-28408.
4 X. Ma, H. Meng, M. Cai and P. K. Shen, *J. Am. Chem. Soc.*, 2012, **134**, 1954-1957.
5 S. Guo, S. Zhang, L. Wu and S. Sun, *Angew. Chem., Int. Ed.*, 2012, **51**, 11770-11773.
6 Y. Liang, H. Wang, P. Diao, W. Chang, G. Hong, Y. Li, M. Gong, L. Xie, J. Zhou, J. Wang, T. Z. Regier, F. Wei and H. Dai, *J. Am. Chem. Soc.*, 2012, **134**, 15849-15857.
7 M. Zhang and L. Dai, *Nano Energy*, 2012, **1**, 514-517.
8 Z. Xiang, Y. Xue, D. Cao, L. Huang, J.-F. Chen and L. Dai, *Angew. Chem., Int. Ed.*, 2014, **53**, 2433-2437.
9 Z. Yang, H. Nie, X. a. Chen, X. Chen and S. Huang, *J. Power Sources*, 2013, **236**, 238-249.
10 W. Wei, H. Liang, K. Parvez, X. Zhuang, X. Feng and K. Muellen, *Angew. Chem., Int. Ed.*, 2014, **53**, 1570-1574.
11 X.-K. Kong, C.-L. Chen and Q.-W. Chen, *Chem. Soc. Rev.*, 2014, **43**, 2841-2857.
12 L. S. Panchokarla, K. S. Subrahmanyam, S. K. Saha, A. Govindaraj, H. R. Krishnamurthy, U. V. Waghmare and C. N. R. Rao, *Adv. Mater.*, 2009, **21**, 4726.
13 C. You, S. Liao, H. Li, S. Hou, H. Peng, X. Zeng, F. Liu, R. Zheng, Z. Fu and Y. Li, *Carbon*, 2014, **69**, 294-301.
14 Z. Yao, H. Nie, Z. Yang, X. Zhou, Z. Liu and S. Huang, *Chem. Commun.*, 2012, **48**, 1027-1029.
15 C. H. Choi, M. W. Chung, H. C. Kwon, S. H. Park and S. I. Woo, *J. Mater. Chem. A*, 2013, **1**, 3694-3699.
16 C. Zhang, N. Mahmood, H. Yin, F. Liu and Y. Hou, *Adv. Mater.*, 2013, **25**, 4932-4937.
17 R. Zheng, Z. Mo, S. Liao, H. Song, Z. Fu and P. Huang, *Carbon*, 2014, **69**, 132-141.
18 K. Gong, F. Du, Z. Xia, M. Durstock and L. Dai, *Science*, 2009, **323**, 760-764.

RSC Advances Accepted Manuscript

 This journal is © The Royal Society of Chemistry 2012

19 J. Wu, D. Zhang, Y. Wang and B. Hou, *J. Power Sources*, 2013, **227**, 185-190.
20 B. Zheng, J. Wang, F.-B. Wang and X.-H. Xia, *Electrochem. Commun.*, 2013, **28**, 24-26.
21 Y. Zhao, L. Yang, S. Chen, X. Wang, Y. Ma, Q. Wu, Y. Jiang, W. Qian and Z. Hu, *J. Am. Chem. Soc.*, 2013, **135**, 1201-1204.
22 Y. Zheng, Y. Jiao, L. Ge, M. Jaroniec and S. Z. Qiao, *Angew. Chem., Int. Ed.*, 2013, **52**, 3110-3116.
23 S. Wang, L. Zhang, Z. Xia, A. Roy, D. W. Chang, J.-B. Baek and L. Dai, *Angew. Chem., Int. Ed.*, 2012, **51**, 4209-4212.
24 L. Wang, P. Yu, L. Zhao, C. Tian, D. Zhao, W. Zhou, J. Yin, R. Wang and H. Fu, *Sci. Rep.*, 2014, DOI: 10.1038/srep05184
25 L. Sun, L. Wang, C. Tian, T. Tan, Y. Xie, K. Shi, M. Li and H. Fu, *RSC Adv.*, 2012, **2**, 4498-4506.
26 Z. Zuo, Z. Jiang and A. Manthiram, *J. Mater. Chem. A*, 2013, **1**, 13476-13483.
27 J. Zhu, C. He, Y. Li, S. Kang and P. K. Shen, *J. Mater. Chem. A*, 2013, **1**, 14700-14705.
28 M. Vikkisk, I. Kruusenberg, U. Joost, E. Shulga, I. Kink and K. Tammeveski, *Appl. Catal., B*, 2014, **147**, 369-376.
29 Z. Lin, G. Waller, Y. Liu, M. Liu and C.-P. Wong, *Adv. Energy Mater.*, 2012, **2**, 884-888.
30 L. Lai, J. R. Potts, D. Zhan, L. Wang, C. K. Poh, C. Tang, H. Gong, Z. Shen, J. Lin and R. S. Ruoff, *Energy Environ. Sci.*, 2012, **5**, 7936-7942.
31 U. B. Nasini, V. G. Bairi, S. K. Ramasahayam, S. E. Bourdo, T. Viswanathan and A. U. Shaikh, *Chemelectrochem*, 2014, **1**, 573-579.
32 H. Wang, X. Bo, C. Luhana and L. Guo, *Electrochem. Commun.*, 2012, **21**, 5-8.
33 T. Xing, Y. Zheng, L. H. Li, B. C. C. Cowie, D. Gunzelmann, S. Z. Qiao, S. Huang and Y. Chen, *Acs Nano*, 2014, **8**, 6856-6862.
34 T. Ikeda, M. Boero, S.-F. Huang, K. Terakura, M. Oshima and J.-i. Ozaki, *J. Phys. Chem. C*, 2008, **112**, 14706-14709.
35 Y. A. Kim, K. Fujisawa, H. Muramatsu, T. Hayashi, M. Endo, T. Fujimori, K. Kaneko, M. Terrones, J. Behrends, A. Eckmann, C. Casiraghi, K. S. Novoselov, R. Saito and M. S. Dresselhaus, *ACS Nano*, 2012, **6**, 6293-6300.
36 Z. Mo, R. Zheng, H. Peng, H. Liang and S. Liao, *J. Power Sources*, 2014, **245**, 801-807.
37 L. Yu, X. Pan, X. Cao, P. Hu and X. Bao, *J. Catal.*, 2011, **282**, 183-190.
38 P. Chen, T.-Y. Xiao, Y.-H. Qian, S.-S. Li and S.-H. Yu, *Adv. Mater.*, 2013, **25**, 3192-3196.
39 J. Chen, X. Wang, X. Cui, G. Yang and W. Zheng, *Chem. Commun.*, 2014, **50**, 557-559.

RSC Advances Accepted Manuscript